An Integrated Approach to Wildland Fire Mapping of California, USA Using NOAA/AVHRR Data

Peng Gong, Ruiliang Pu, Zhanqing Li, James Scarborough, Nicolas Clinton, and Lisa M. Levien

Abstract

To map wildland fires for emission estimation in California, this paper presents an integrated approach to wildfire mapping using daily data of the Advanced Very High Resolution Radiometer (AVHRR) on board a National Oceanic and Atmospheric Administration's (NOAA) satellite. The approach consists of two parts: active fire detection and burnt area mapping. In active fire detection, we combined the strengths of a fixed multi-channel threshold algorithm and an adaptive-threshold contextual algorithm and modified the fire detection algorithm developed by the Canada Center for Remote Sensing (CCRS) for fire detection in boreal forest ecosystems. We added a contextual test, which considers the radiometric difference between a fire pixel and its surrounding pixels, and a sun glint elimination test to the CCRS algorithm. This can effectively remove false alarms caused by highly reflective clouds and surfaces and by warm backgrounds. In burnt area mapping, we adopted and modified the Hotspot and NDVI Differencing Synergy (HANDS) algorithm, which combines the strengths of hotspot detection and multi-temporal NDVI differencing. We modified the HANDS procedure in three ways: normalizing post-fire NDVI to pre-fire NDVI by multiplying an NDVI ratio coefficient, calculating mean and standard deviation of NDVI decrease of land-cover types separately, and adding a new iteration procedure for confirming potential burnt pixels. When the integrated method was applied to the mapping of wildland fires in California during the 1999 fire season, it produced comparable results. Most of the wildfires mapped were found to be correct, especially for those in forested ecosystems. Validation was based both on limited ground truth from the California Department of Forestry and Fire Protection and on interpreted burnt areas from Landsat 7 TM scenes.

Peng Gong and Ruiliang Pu are with the State Key Lab of Remote Sensing Science, IRSA, Box 9718, Beijing, China, 100101 (gong@nature.berkeley.edu).

Peng Gong, Ruiliang Pu, James Scarborough, and Nicolas Clinton are with the Center for Assessment and Monitoring of Forest and Environmental Resources, 137 Mulford Hall, University of California, Berkeley, CA 94720.

Zhanqing Li is with the Department of Meteorology and Earth System Science Interdisciplinary Center, University of Maryland, College Park, MD 20742-2465.

Lisa M. Levien is with the USDA Forest Service, Forest Health Protection, 1920 20th Street, Sacramento, CA 95814.

Introduction

Wildfires and prescribed burning occur frequently in California. They produce hazardous emissions leading to episodic increases in particulate matter ($PM_{2.5}$) and visibility reducing particles. Smoke from such burning, if not properly managed, can have significant health impacts on exposed populations. A reliable estimation of burnt areas caused by biomass burning in California, therefore, is a key for emission estimation. Ground-based measurements of fire perimeters after-fire events or regular overpasses for fire mapping during the burning using an airplane with an onboard sensor may not meet the requirement for emission estimation at a regional or continental scale. Remote sensing is the most efficient and economic means for monitoring fires over large areas on a routine basis despite its various limitations (Li *et al.*, 2000a, b; Justice *et al.*, 1993). The type of sensor most widely used for long-term, large-scale fire monitoring is the Advanced Very High Resolution Radiometer (AVHRR) on board the National Oceanic and Atmospheric Administration's (NOAA) polar orbiting satellites (Stroppiana *et al.*, 2000; Li *et al.*, 1997; Justice *et al.*, 1996; Kennedy *et al.*, 1994; Kaufman *et al.*, 1990; Flannigan and Vonder Haar, 1986).

AVHRR (onboard the NOAA-14 satellite and earlier) data are available at a nominal spatial resolution of 1.1 km in five channels: the visible, near-infrared (IR), mid-IR, and two thermal-IR portions of the spectrum. Such spectral resolution offers considerable benefits to fire monitoring (Harris, 1996). Channels 1 and 2 provide data capable of detecting, monitoring, and measuring smoke emissions (Khazenie and Richardson, 1993; Kaufman *et al.*, 1990), but contain no thermal information. Channel 3 is extremely sensitive to sub-pixel hot spots, making it the most important channel for fire detection (Rauste *et al.*, 1997; Pozo *et al.*, 1997; Franca *et al.*, 1995; Setzer and Pereira, 1991; Muirhead and Cracknell, 1985) though it has a low temperature saturation point (~321 k) (most existing algorithms concentrate on the third channel, hoping to overcome this disadvantage). Channels 4 and 5 are far less sensitive to sub-pixel hotspots, but they can frequently help detect fires when combined with other channels (Flasse and Ceccato, 1996; Justice *et al.*, 1996). In addition, the AVHRR onboard post-NOAA-14 satellites also include a 1.65 μm short wave infrared (SWIR)

Photogrammetric Engineering & Remote Sensing
Vol. 72, No. 2, February 2006, pp. 139–150.

0099-1112/06/7202–0139/$3.00/0

channel. The SWIR channel has been proven highly effective in discriminating burned boreal forest (e.g., Fraser and Li, 2002).

Wildfire mapping using NOAA/AVHRR data involves active fire detection, as well as burn scar mapping. Existing AVHRR-based fire detection algorithms can be grouped into two broad categories: (a) fixed threshold algorithms; and (b) adaptive threshold contextual algorithms (Giglio *et al.*, 1999). Fixed threshold algorithms apply empirically-determined thresholds to discriminate fire pixels from their non-burning surroundings or from clouds (Boles and Verbyla, 2000). Threshold values are defined and fixed for given regions and seasons. Flannigan and Vonder Haar (1986) first used the fixed threshold method to identify fire pixels. If the temperature for both channel 3 and channel 4 exceeded the mean background temperature, and if channel 3 was greater than channel 4 by a critical threshold, fire was assumed to exist. They detected 80 percent of unobstructed fires. Kaufman *et al.* (1990) used a threshold-based fire detection method in an assessment of trace gases and particulate emission from fires in Brazil. They found that lower threshold values resulted in an increased number of false fire detections caused by warm surface areas. Kennedy *et al.* (1994) modified the threshold set by Kaufman *et al.* (1990) using AVHRR data for West Africa and improved fire detection effectiveness. Li *et al.* (1997; 2000a), Rauste *et al.* (1997), Pozo *et al.* (1997), and Arino and Melinotte (1998) employed fixed multiple thresholds applied to multiple channels to detect active fires in the Canadian boreal forests, Spain and Africa, respectively. The fire detection studies cited above achieved varying degrees of success. The advantages of this category of algorithms for active fire detection are simplicity and reduction of computation time. The limitation of this method is that the fixed thresholds are only applicable at local to regional scales during a short fire season.

Instead of using fixed threshold values throughout an area, a category of contextual algorithms using adaptive thresholds was proposed. The algorithms compute variable, pixel-specific thresholds based on the pixels surrounding a potential fire pixel. Flexible threshold algorithms identify a fire pixel based on the level of contrast between the potential fire pixel and its "background" pixels (the definition of background varies with kernel size; Boles and Verbyla, 2000). Contextual algorithms are designed to be flexible, and effective under different environmental conditions (Flasse and Ceccato, 1996). Lee and Tag (1990) proposed one of the first contextual fire detection algorithms in their analysis of gas waste flares from AVHRR nocturnal data. A contextual algorithm adapted from Flasse and Ceccato (1996) was used for the International Geosphere Biosphere Program, Data and Information Systems (IGBP-DIS) fire product (Stroppiana *et al.*, 2000; Dwyer *et al.*, 1998; Malingreau and Justice, 1997; Justice and Dowty, 1994). Contextual methods have also been used for regional fire monitoring, such as over central Africa (Eva and Flasse, 1996). In principle, contextual methods are more versatile, being able to handle a wider range of conditions than the fixed threshold approaches. It should be noted that if a set of thresholds were set too high to distinguish between potential fire pixels and background non-fire pixels, a large omission error would occur. Since the fire confirmation tests employed in subsequent contextual algorithms work only on potential fire pixels so identified, the omission error problem could then only get worse (Li and Giglio, 1999). Therefore, when a contextual algorithm is employed, it is necessary to pay close attention to setting initial thresholds for identifying potential fire pixels.

Active fire detection as described above covers only a portion of a region's total burnt area in any given season, due to clouds and limitation in satellite over-pass frequency (Li *et al.*, 2000b; Eva and Lambin, 1998a). Burn scar mapping overcomes this problem, providing complete mapping and statistics on burnt areas. Extraction of burnt land information from AVHRR data can be done using any of the following three approaches: (a) application of multiple tests on spectral values or on derived indices based on single date data; (b) temporal analysis; and (c) classical image segmentation techniques with single date or multi-temporal data (Arino *et al.*, 1999). All approaches require a post-fire image. In the first approach, burn scars can be detected based on the spectral difference between burnt and un-burnt areas in individual channels and/or in a combination of channels (e.g., NDVI; Pereira, 1999; Razafimpanilo *et al.*, 1995). In the second approach, changes caused by fire activity are tracked for burn scar mapping. For example, Kasischke and French (1995) used AVHRR data taken before and after a large forest fire in Alaska to map burn scars based on a post-fire decrease in NDVI. Fernandez *et al.* (1997) and Martin and Chuvieco (1995) also applied pre- and post-fire NDVI differences to map burn scars. It has been demonstrated that this method is more effective than methods using only a single post-fire image, since the second method minimizes potential confusion with permanent land cover types, some of which have spectral patterns similar to fire scars (Pereira *et al.*, 1997). The third type of method involves image classification and post-classification comparison. Recently, a new type of burn-scar mapping algorithm has been proposed that combines an active-fire detection algorithm with NDVI and/or other vegetation index differencing (Pereira 1999). For example, one technique, known as Hotspot and NDVI Differencing Synergy (HANDS), combines the strengths of its two constituent techniques while avoiding their limitations (Fraser *et al.* 2000).

Recently, the Moderate Resolution Imaging Spectroradiometer (MODIS), onboard EOS series satellites) imagery has become another source of data of appropriate spatial and temporal resolution to be used for global studies of biomass burning (Kaufman *et al.* 1998a). These active-fire detection and burnt scar mapping algorithms, briefly reviewed above, can be modified and applied to MODIS data.

In this study, the CCRS active fire detection algorithm (Li *et al.*, 2000a) was modified with additional contextual and sun glint tests, and used to detect daily hotspots in California using NOAA/AVHRR data. Then, the HANDS procedure (Fraser *et al.*, 2000) was modified and used for mapping burn scars in California, using NDVI differencing and a hotspot mask covering an interesting time period. Therefore, to obtain a reliable estimation of burn scars covering a variety of fuel types in California, we propose in this study an integrated approach for mapping wildfires with the NOAA/AVHRR data. The objectives in this study are to integrate the use of contextual information into the multi-channel fixed threshold algorithm (Li *et al.*, 2000a) for hotspot detection, and to adopt and modify the HANDS algorithm (Fraser *et al.*, 2000) for burn scar mapping.

Data Sources

Daily High Resolution Picture Transmission format (AVHRR-HRPT) images (1.1 km resolution at nadir) from 01 May to 31 October 1999 were acquired on board the NOAA-14 satellite during its daytime passes. The local passing time of NOAA-14 over California varied from 1400 to 1600 hours (local time). Due to excessive cloudiness and a data acquisition problem, a total of only 148 daily images were available for this analysis (missing nine days in May, ten days in June, eight days in July, four days in August, one day in September, and four days in October). In order to generate

ten-day maximum value composite, NDVI = (Ch2 − Ch1)/(Ch2 + Ch1) (MVC-NDVI) composite images for October 1998, an additional ten daily of AVHRR-HRPT images acquired from 21 to 31 October 1998 were used. The daily NOAA/AVHRR data used in this study were downloaded from NOAA Satellite Active Archive Data Center (**http://www.saa.noaa.gov**). In this study, previously mapped land cover types of California were used to eliminate non-wildland cover types and to calculate NDVI difference statistics within each cover type, needed for hotspot detection and burn scar mapping. The Gap Analysis Project (GAP) vegetation data set (Holland, 1986; Anderson *et al.*, 1976) was used as our land-cover type map. It was compiled from multiple sources, relying primarily on 1990 Landsat TM data, for evaluation of habitat and land conservation. The land-cover types used for fire detection and mapping consist of scrub and chaparral, grassland, marsh, riparian forest and scrub, woodland and rangeland, forests, and fell-field.

Three Landsat-7 TM scenes (path45/row32, path44/row32, and path44/row33) were acquired on 03 November, 12 November, and 12 November 1999, respectively. And a partial data set of fire polygons collected by the California Department of Forestry and Fire Protection (CDF) through ground survey was used to validate our results.

Methods

AVHRR Data Preparation

The PACE AVHRR Orbital Navigation Package (PCI Geomatics Company, Canada, 1997), a module specially designed for pre-processing NOAA/AVHRR data, was used to perform AVHRR data preparation using calibration and orbit information and extracted ground control points from the AVHRR data file. Geometric correction and registration were accomplished. The entire data preparation involved five steps:

1. Data Download and Import. The AVHRR data format used in this analysis is HRPT. The data were downloaded directly from **http://www.saa.noaa.gov**. Normally, all five AVHRR channels were read in.
2. Radiometric Correction. The scan angle of the AVHRR sensor is large (approximately 110.8 degrees), so there is a range of solar zenith angles along any given scanline. Therefore, different parts of an AVHRR image receive differing amounts of solar radiation. The imbalance can be removed by performing a radiometric (solar zenith angle) correction (Di and Rundquist, 1994). This correction was performed on AVHRR channels 1 and 2.
3. Radiometric Calibration. Digital numbers (DN) of AVHRR data must be converted to standard physical units. The outputs are expressed as percent reflectance from the top of the atmosphere (TOA) for Channels 1 and 2, and as brightness temperature in K from the TOA for the thermal channels.
4. Geometric Correction. All five AVHRR channels were geocorrected. The correction procedure applies the information extracted from the raw AVHRR data file during the data import process to automatically rectify all five calibrated AVHRR channels. The resulting pixel size is 1 km. The georeferencing error of an image after this step may be greater than two pixels.
5. High Precision Geometric Correction and Registration. This was achieved using six to ten manually collected ground control points (GCPs). The georeferencing error at this stage was less than 1 km.

Hotspot Detection Algorithm

The active fire detection algorithm is based on the algorithm of Li *et al.* (2000a, hereafter called the CCRS algorithm) with a modification for California. This algorithm was chosen based on the comparison of results from five fire detection algorithms (Li *et al.* 2001). The five algorithms under study include four designed for global applications and one designed specifically for boreal forests. The global algorithms include one used in generating the IGBP-DIS fire product (Malingreau and Justice, 1997), one designed for the MODIS (Kaufman *et al.*, 1998a; 1998b), one employed at the European Space Agency (ESA) (Arino *et al.*, 1998), and one proposed by Giglio *et al.* (1999). The regional algorithm was developed and first operated at the Canada Center for Remote Sensing (CCRS) (Li *et al.*, 2000a). Two of the algorithms use fixed thresholds (CCRS and ESA) and three use contextual methods with variable thresholds (IGBP, MODIS, and Giglio *et al.*, 1999). The comparison result indicates that the CCRS algorithm is best for large area fire detection over Canada's boreal forest (Li *et al.*, 2001). However, since the CCRS algorithm was originally designed for boreal forests and temperate areas, with fixed threshold tests built in to the algorithm, we added some new tests to deal with the diversity of environments in California. The tests are divided into two major stages: identifying potential fire pixels and eliminating false fires. At the second stage, eliminating false fires, we added a function for false alarm removal that considers background effects. As in the CCRS algorithm, thresholds of all tests were optimized for real fire detection by eliminating as many false fires as possible. The threshold values were chosen following a trial-and-error approach based on the fire training data sets from CDF fire polygons. The schematic representation (Figure 1) of the spectral correspondence of several known land-cover types, particularly hotspot and burn scar, helped us in the threshold determination. From Figure 1, it is easy to see that hotspot and burn scar types have a certain level of intersection in the spectral space, and also that they overlap with other land-cover types to a certain degree. Identification of fire pixels is difficult if only a few tests are done. The multi-channel threshold algorithm that considers surrounding pixel effects is summarized in a flowchart (Figure 2).

In Figure 2 (note that brightness temperature channels 3, 4, and 5 are hereafter denoted as T3, T4, and T5, and reflectance channels 1 and 2 are, hereafter, denoted as R1 and R2), as in most previous work (Li *et al.*, 2000a; Li and Giglio, 1999; Arino and Melinotte, 1998; Justice *et al.*, 1996; Franca *et al.*, 1995; Kennedy *et al.*, 1994), AVHRR T3 (centered around 3.7 μm), which catches all potential fire pixels, is used first. The threshold for T3 was selected based on the assumption that fires at sub-pixel levels will generate a temperature that approaches the channel saturation point (~320K, in this study, it is 322K). Since the middle-infrared channel is very sensitive to thermal radiation, this assumption is reasonable given the low saturation point (Justice *et al.*, 1996). Most wildfires have a large range of burning temperatures, from approximately 500K for smoldering fires to over 1,000K for flaming fires, with a variable fraction of the burning area being within any given pixel (Kaufman *et al.*, 1998). However, since the AVHRR sensor was not designed for fire detection, it loses sensitivity at such high temperatures. Nevertheless, because the brightness temperature for most fire-free pixels is usually significantly lower, it still proves to be the most useful channel for fire detection. For potential fire identification, Li *et al.* (2000a) used a threshold of 315K in boreal forests and Kaufman *et al.* (1990) used 316K in tropical forests. We chose 315K in this study.

At the second stage, all tests are for removing false fires after the initial potential fire detection. The thresholds chosen for tests 2, 3, 5, 6, and 9 were kept the same or close to the corresponding tests in the CCRS algorithm (Li *et al.*, 2000a). The threshold of test 2 (T3-T4), for testing the brightness-temperature difference between AVHRR channels 3

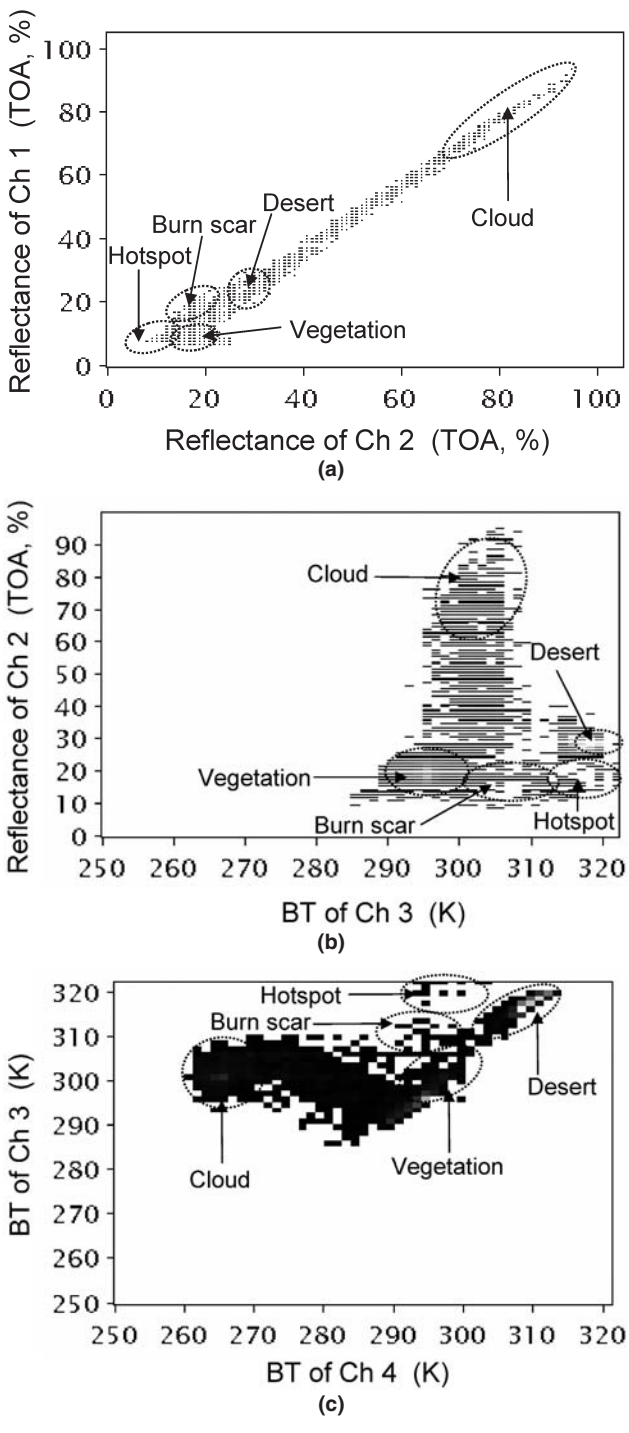

Figure 1. Schematic representation of the spectral correspondences of several land cover types (each approximately within a dotline ellipsis). (a) Distribution of reflectance values from the top of atmosphere (TOA) for channels 1 and 2; (b) distribution of reflectance from the TOA in channel 2 and brightness temperature in channel 3; and (c) distribution of brightness temperature for channels 3 and 4.

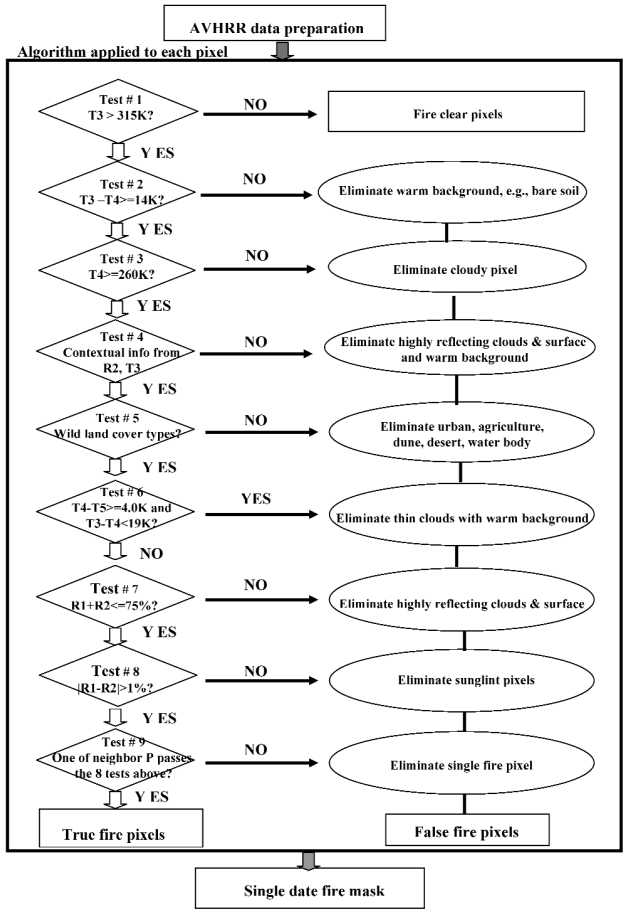

Figure 2. A flowchart of hotspot detection using NOAA-14/AVHRR data presents a process-chain to produce an active fire.

and 4, was set at 14K. Its function is to eliminate false fires caused by warm backgrounds such as bare soils, because these types of warm backgrounds can saturate channel 3. It is known that in the case of biomass burning, the value of T3-T4 is high (Li *et al.*, 2000a; Kennedy *et al.*, 1994). Test 3 (set T4 >= 260K) eliminates those pixels containing highly reflective clouds. Although test 1 (T3 > 315K) can filter out heavily clouded pixels, many bright or highly reflective cloud pixels may be missed. The purpose of test 5 is to focus hotspot detection on wilderness areas. Test 6 eliminates false fire pixels caused by thin cirrus clouds and removes the false fires caused by warm backgrounds passing previous tests. The ninth test limits confirmed fire pixels not surrounded by another fire pixel within a 3×3 window. It is assumed that in most cases single fire pixels are caused by sub-pixel contamination and other noise, such as a forest pixel containing a fraction of water body with an insufficient amount of sun glint to be eliminated by test 8.

Despite our attempts to adjust thresholds for various tests in the CCRS algorithm based on the limited data set of fire polygon data (CDF), there remained many false alarms. In consideration of the difference between the relatively "cold background" of the Canadian boreal forests, the relatively "warm background" of northern California, and the "hot background" of southern California brush land, and considering as well the sun glint problem caused by the coastline and many inner lakes of California, we added three more tests to remove the remaining false fires. Tests 4, 7, and 8 were added to the CCRS algorithm. In addition to the R2 < 22 percent threshold, effects of surrounding pixels on the

central pixel in AVHRR channels 2 and 3 (R2 and T3) were taken into consideration. Test 4 for R2 involves the following assessment: if R2 $<$ 22 percent, then the subtest is passed; if R2 $>$ 30 percent then there is no fire; if R2 is between 22 percent and 30 percent, and R2 $<$ the mean of its eight surrounding pixels minus 1.0 percent, then the subtest is passed. When R2 is between 22 to 30 percent, there are two possible scenarios for the vegetated pixel. The first is partial burning within a pixel at the canopy or ground level. In this case, it is likely that the NIR reflectance, R2, of that pixel does not drop to below 22 percent. Nevertheless, R2 is dramatically lower than the R2 of surrounding pixels (e.g., most normal forest vegetation has greater than 30 percent reflectance for R2). In the second scenario, non-fire pixels may fall into the range of 22 to 30 percent, but their R2s are equal or close to those of their surrounding pixels. Therefore, the subtest can retain a fire pixel and remove a false alarm. Test 4 for T3 is as following: if T3 is greater than the mean of its eight surrounding pixels +5K, then the subtest is passed. If a pixel is composed of varied proportions of "warm" and "cold" components (e.g., bare soil and water body), it is possible for the pixel to pass Test 2 (Li *et al.*, 2001). However, if the T3 value of the pixel is similar to the values of its surrounding pixels, then the pixel is considered a false fire, and removed. In the above test, if any one of the eight surrounding pixels is a potential fire pixel, it will be temporarily replaced by the average pixel value of the land cover type to which it would have belonged before the fire. Test 4 can effectively remove false fires caused by highly reflective clouds, bright surfaces and warm backgrounds. The newly added test 7 is designed to further eliminate highly reflective clouds and bright surfaces. At particular sun-earth-satellite geometric configurations, sun glint on water causes the algorithm to falsely detect fire. This problem is common along coastlines, but also among inland water-logged areas such as irrigated regions, marshes, and lakes of various sizes (Malingreau and Justice, 1997). Such land types are common in California. Although such land types are masked out by test 5, registration error (usually subpixel error) still can cause such a sun-glint problem. Since the values of R1 and R2 are very close to each other over a sun glint pixel, test 8 was designed to remove sun glint pixels.

Table 1 provides a complete comparison of all tests for the two algorithms designed by CCRS and us. Although the original CCRS algorithm already had steps for dealing with most of the effects of surrounding pixels, sun glint, and highly reflective clouds and surfaces on a potential fire, they did not work well in the wide variety of temperate biomes in California. Therefore, we added into the algorithm the three tests described above.

TABLE 1. COMPARISON OF ALGORITHMS USED FOR HOTSPOT DETECTION BY OURS AND CCRS

CCRS (NOAA-14)	Ours (NOAA-14)
T3 $>$ 315 K	T3 $>$ 315 K
T3 $-$ T4 $>$ 14 K	T3 $-$ T4 $>=$ 14 K
T4 $>$ 260 K	T4 $>=$ 260 K
R2 $<$ 22%	R2 $<=$ 22%
n/a	If 22% $<$ R2 $<=$ 30% and R2 $<$ (mean of 8 neighbor pixels -1), then fire; if R3 $>$ (mean of 8 neighbor pixels +5), then fire.
Eliminate cropland, grassland and water bodies	Eliminate water bodies, urban, agricultural area dune and desert.
T4 $-$ T5 $<$ 4.1K and T3 $-$ T4 $>=$ 19K	T4 $-$ T5 $<$ 4K and T3 $-$ T4 $>=$ 19K
n/a	R1 + R2 $<=$ 75%
n/a	$\lvert R1-R2 \rvert > 1\%$
Eliminate single pixel fires	Eliminate single pixel fires

Burnt Area Mapping

To assess burnt areas during a fire season in California, a multi-temporal NDVI differencing technique was selected. We adopted the rationale of the HANDS procedure (Fraser *et al.*, 2000) for mapping burnt areas in California and modified it. The three major modifications to the HANDS algorithm (Fraser *et al.*, 2000) are described in the following.

NDVI Composite Normalization (Step 1 in Table 2)

To compensate for any systematic NDVI variation unrelated to fire, post-fire NDVI (NDVIPOST) composites were normalized to the pre-fire NDVI (NDVIPRE) composite. This was done by calculating a ratio, Ratio_C,

$$\text{Ratio\_C} = \text{Average of NDVIPRE}/\text{Average of NDVIPOST}. \quad (1)$$

Hotspot pixels were excluded from the calculation. NDVIPOST is then rescaled by Ratio_C:

$$\text{NDVINORM-POST}(i,j) = \text{Ratio\_C} * \text{NDVIPOST}(i,j). \quad (2)$$

NDVI variation is associated with seasonal or inter-annual variation of vegetation phenology, depending on the time interval between NDVI composites (Kasischke and French, 1997). The differences between NDVIPRE (NDVI MVC of 21–31 October 1998) and NDVIPOST (NDVI MVC of 21–31 October 1999) of seven land cover types demonstrate this

TABLE 2. A SUMMARY OF THE MODIFIED HANDS ALGORITHM

Step	Description
Step 0	AVHRR data preparation: two NDVI composites of an interesting interval, one corresponding hotspot composite (fire mask)
Step 1	Normalize NDVIPOST to NDVIPRE: means of NDVIS calculated only with interested land covers $\text{Ratio C} = \frac{\text{mean of NDVIPRE}}{\text{mean of NDVIPOST}}$, normalized NDVIPOST = Ratio.C * NDVIPOST, not hotspot pixels used for calculation of NDVI mean.
Step 2	Calculate NDVI difference: normalized NDVIPOST – NDVIPRE, burn scar expected to have a negative value in the NDVI difference image.
Step 3	Confirm hotspot pixels (CBP) using NDVI difference: a CBP is assumed to have a negative NDVI difference, otherwise the hotspot pixel is considered as a false fire.
Step 4	Calculate NDVI difference statistics (mean, standard deviation, SD) of NDVI decrease for all CBPs for each land cover type, different land covers expected to have a different mean and SD.
Step 5	Select potential burn scar pixels (BSPs): NDVI difference of a potential BSP $<$ (mean + 0.5SD), the potential BSPs selected for different land cover types with the mean and SD from Step 4.
Step 6	Apply a sieve filter to the selected BSPs: filter out a burnt patch of $<$3 pixels, a burn patch less than 3 pixels is considered to be caused by noise.
Step 7	Confirm a BSP with a neighbor CBP and later on up to four neighbor confirmed BSPs to create connected burn patches, 1st iteration with a neighbor CBP, 2nd iteration with a neighbor CBP or a conformed BSP (CBSP), 3rd to 5th iteration with 2 to 4 CBSPs, after 5th iteration using 4 CBSPs only.
Step 8	Filter out a BSP patch of $<$3 pixels: the patch of $<$3 CBSPs is considered to be a false burnt patch, caused by noise.
Step 9	Output a burnt area mask (in TIFF format).

TABLE 3. STATISTICS OF PRE-FIRE NDVI MVC AND POST-FIRE NDVI MVC AS WELL AS NDVI DECREASES ACROSS SEVEN LAND-COVER TYPES RELATED TO WILDLAND FIRES

Item	Total Mean/SD	Means (/SD)						
		Scrub, Chaparral	Grassland	Marsh	Riparian, Forest, Scrub	Woodland, Rangeland	Forests	Fell-Field
NDVIPRE	166.587/21.064	152.92	158.16	165.22	147.48	169.37	189.24	151.01
NDVIPOST	164.495/21.665	150.36	154.46	161.56	145.75	167.10	188.45	148.98
NDVIPOST*Ratio_C	166.587/22.087	152.27	156.42	163.61	147.60	169.23	190.85	150.87
NDVIPOST + Difference	166.495/21.665	152.36	156.46	163.56	147.75	169.10	190.45	150.98
NDVIDECREASE	123.327/4.444	123.95/3.75	122.46/3.72	120.73/5.04	124.45/3.55	123.04/4.39	122.49/5.94	123.43/3.43

Note: a) Ratio_C = Mean(NDVIPRE)/Mean(NDVIPOST) = 1.0127; Difference = Mean(NDVIPRE) – Mean(NDVIPOST) = 2.092.
b) A real NDVI value = (value in the table – 127.5)/127.5.
c) NDVIPRE and NDVIPOST are NDVI MVC of 21–31 October 1998 and 1999, respectively.

variation (Table 3). Therefore, it is necessary to conduct such normalization before analyzing NDVI change related to biomass burning. Fraser *et al.* (2000) calculated the difference between the two averages of NDVI composites, and then added the difference to the post-fire NDVI. This method ensures that both NDVI composites have the same average. We multiplied a ratio by the NDVI value for each post-fire pixel. This allowed us to realize the normalization of the post-fire NDVI composite. This multiplicative factor thus ensures that the rescaled values are proportionally adjusted.

Calculate NDVIDIFF Statistics (Step 4 in Table 2)
The mean and standard deviation (SD) of NDVI decreases for all confirmed burning pixels (CBPs) were calculated separately for each land-cover type. Unlike the boreal forests addressed by Fraser *et al.* (2000), who did not separately calculate the mean and SD for each land cover type, our dataset demonstrates that the magnitude of NDVI change varies with different types of land cover in California (see NDVIDECREASE in Table 3). For example, NDVI decreases are very different between forest types (mean = 122.49/SD = 5.94) and marsh types (mean = 120.73/SD = 5.04). Note that the values in Table 3 have been scaled from NDVI [−1, 1] to NDVI [0,255] for display purposes. Therefore, separately calculating the mean and SD of NDVI decreases may be expected to increase burn scar mapping accuracy.

Confirm a Potential BSP (Burn Scar Pixel) (Step 7 in Table 2)
Potential BSPs are confirmed iteratively. A BSP is confirmed by a neighbor CBP or later on by one to four previously confirmed neighbor BSPs. The first iteration is executed by a neighbor CBP; the second iteration by a neighbor CBP or a confirmed BSP; the third to fifth iteration by two to four confirmed BSPs; and after the fifth iteration by four confirmed BSPs only. This modification is not only for easily realizing the iteration process, but also is expected to grow boundaries of burn scars more smoothly.

The processing chain, presented above and summarized in Table 2, is fully automated using a script in EASI® programming (PCI Geomatics Company, Canada, 1997). The results from critical steps are illustrated in Figure 3 and will be analyzed in the following section. If the goal is to map cumulative burnt area during a fire season, the time span is first divided into several periods each corresponding to an available hotspot composite mask. Steps 1 through 9 can then be repeated to create a burnt area map for each period. Finally, results in each period can be overlaid together to derive a burnt area map for the fire season. In this study, we used the entire fire season of 1999 in California as one time interval corresponding to 01 May through 31 October 1999.

Validation

The ground truth data for the 1999 fire season from CDF were incomplete for California. In the data set, the accuracy of fire polygon locations varied. Some polygons were missing data for the date of fire emergence and for fire acreage. Therefore, three Landsat-7 TM scenes acquired in early November of 1999 were used to delineate some obvious burnt patches to help validate the burn scar mapping results derived from AVHRR data. We simply compared burnt areas from AVHRR mapping results with those delineated by TM scenes and provided by CDF.

Results and Analysis

Hotspot Detection

The hotspot detection algorithm was applied to detect hotspot pixels using a total of 148 daily AVHRR images, covering six months and the entire state of California. A monthly fire mask was composed of daily hotspot masks for each month. Plate 1 shows a sub-area of the four-month fire mask composite for northern California. Plate 1a shows three active fires, occurring on 02 September 1999 in northern California. The fires are marked in red circles, with a background of the AVHRR composite image (R2/R2/R1 versus RGB). Comparing the results (Plate 1b) produced by the CCRS algorithm with those (Plate 1c) produced by our modified algorithm, we see that the CCRS algorithm generated many "salt and pepper" hot spots, which are obviously false alarms. During the four-month period spanning almost an entire fire season of 1999 in California, the CCRS algorithm produced 14,281 active fire pixels, while the modified algorithm generated only 1,124. The result obtained from the modified algorithm looks reasonable compared with an independent burnt area estimation of 3,500 to 4,000 km^2 in California in 1999 (refer to an incomplete fire polygon data set (3,205 km^2) from CDF in 1999). Fires can be identified visually by co-locating hot spots on the channel 3 image with the associated smoke plume patterns on channel 1 (Li *et al.*, 1997; Setzer and Malingreau, 1996). On a composite image (R2/R2/R1 versus RGB, see Plate 1a), a smoke plume accompanying a fire usually exhibits a conical or bending shape with a vortex over its origin (Li *et al.*, 2000a). Visual inspections indicated that most of the fires detected by our algorithm were correctly identified. An inspection of available fire polygons provided by CDF also indicated that most of the hot spots were located in those fire polygons, though there were a few hot spots located outside. The CCRS algorithm, applied in California, generated many false fires. This may be explained by two factors. First, the CCRS algorithm was designed for fire detection in boreal forests

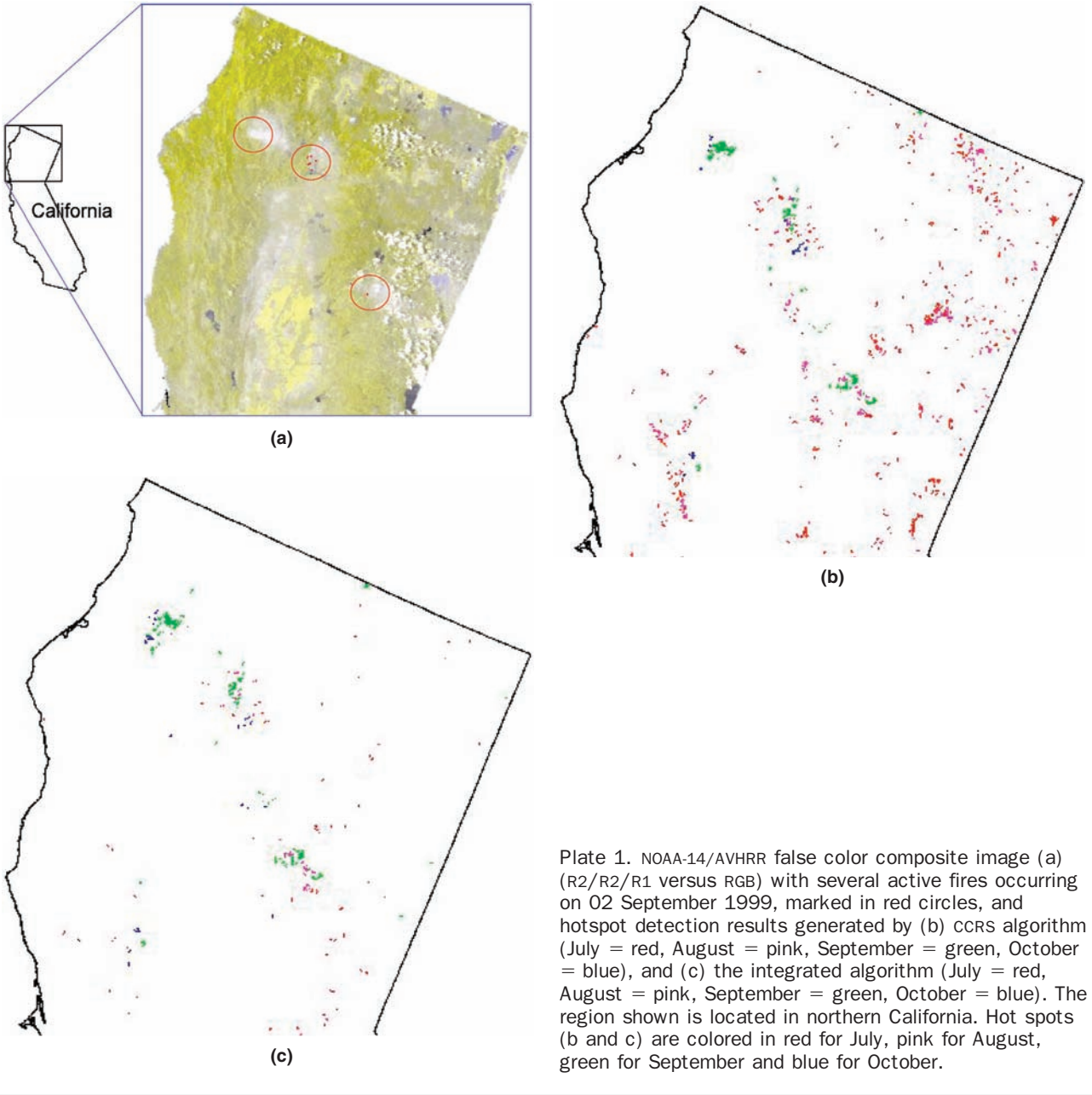

Plate 1. NOAA-14/AVHRR false color composite image (a) (R2/R2/R1 versus RGB) with several active fires occurring on 02 September 1999, marked in red circles, and hotspot detection results generated by (b) CCRS algorithm (July = red, August = pink, September = green, October = blue), and (c) the integrated algorithm (July = red, August = pink, September = green, October = blue). The region shown is located in northern California. Hot spots (b and c) are colored in red for July, pink for August, green for September and blue for October.

with a "cold background", while Californian forests have a "warm background." Therefore, if the CCRS algorithm is simply applied to California with no modifications, false fires caused by warm backgrounds, such as bare soil, are inevitable. Secondly, the CCRS algorithm does not consider the effects of sun glint on fire detection. Sun glint may not be a problem for boreal forests at higher latitudes, but for California it becomes a problem because California has a longer coastline and inner lakes that frequently cause sun glint, especially when the sensor viewing zenith is close to the solar zenith (Rauste *et al.*, 1997).

Burnt Area Mapping

After hotspots (monthly fire composites, color-coded in Plate 1c) were obtained, burn scars could be mapped. Two ten-day NDVI composites were calculated before running the modified HANDS procedure for mapping burn scars (in Table 2) with data from the 1999 fire season in California: Pre-fire and post-fire NDVI MVCs were calculated with the period of 21–31 October 1998 and 1999, respectively.

To demonstrate the effectiveness of the modified HANDS procedure for the detection of burn scars, Figure 3 presents the mapped results from September 1999, using pre-fire NDVI MVC (01–10 September) and post-fire NDVI MVC (01–10 October) and the hotspot composite for September. Figure 3a shows a part of the NDVI difference image set in between the normalized post-fire and the pre-fire NDVI composites. On this image, burn scars were assumed to have an NDVI decrease. At the upper left of the image, a light patch caused by a plume of burning smoke occurred nearly every day during 01–10 September, while the burning stopped almost completely during the period of 01–10 October. A dark gray area at the central bottom of the image is agricultural land, which yields low NDVI composite values and is excluded

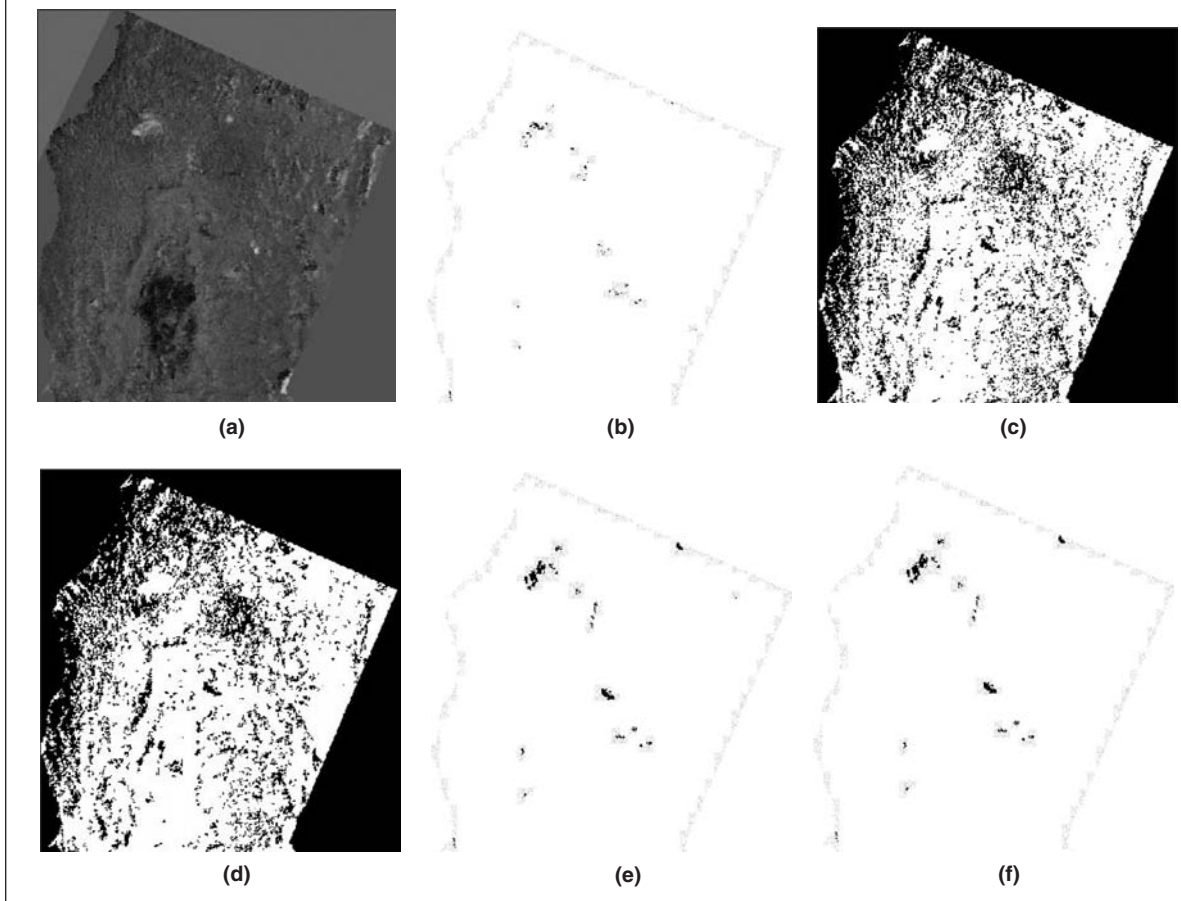

Figure 3. Results derived from key steps (Table 2) of the modified HANDS burn scar-mapping algorithm. The region shown is the same as in Plate 1. (a) Steps 1 and 2, NDVI difference calculation between the normalized post-fire and the pre-fire NDVI composites; (b) Step 3, confirmed hotspots (CBP) using NDVI decrease; (c) Steps 4 and 5, calculation of potential burn scar pixels (BSPs) for each land cover type based on 0.5 SD added to the mean NDVI decrease of CBPs; (d) Step 6, filtering of burnt patches smaller than two pixels; (e) Step 7, confirmed potential BSPs burnt patch generation; and (f) Step 8, filtering confirmed burnt patches smaller than two pixels based on results presented in (e).

from the wildfire map. Figure 3b is the confirmed burning pixel (CBP) map on which the CBP was determined using the assumption that a real burning pixel has to be accompanied by an NDVI decrease. Most CBPs at the upper left of the image are located in the anterior sections of smoke areas shown in Figure 3a (upper left). There are a large number of potential burn scar pixels (BSPs) in Figure 3c. Among them, only a small portion is actually due to fires. The solar-elevation change and phenological changes between early September and early October may be responsible for the large number of false alarms. Figure 3d shows the effectiveness of filtering for removal of burnt patches smaller than two pixels. Figure 3e illustrates the usefulness of a confirmation approach with various numbers of confirmed neighbor BSPs and a neighbor CBP. Only a small number of burn scars remain after using the confirmation approach. Figure 3f shows the same effect as Figure 3d.

Figure 4 presents a section of burn scar mapping after application of the modified HANDS algorithm. The map (total 3,473 km^2) covers the 1999 fire season in California using a hotspot composite of 01 May to 31 October and two NDVI MVCs of 21–31 October 1998 and 1999, respectively. In general, the distribution and magnitude of burn scars mapped by the algorithm are seen to be reasonable when compared to an incomplete CDF data set and TM interpretation results, especially for major fire events in forest ecosystems. In order to evaluate and gain insight into the burn scars detected by the algorithm, we selected four major burnt areas, each one representative of a major fuel type (ecosystem) of California. The fire polygons of the four burnt areas were available from CDF data set. The black lines in Figure 5 represent fire polygon boundaries and the light shadow areas inside and outside the polygons are burnt areas detected by the algorithm. The region mapped in Figure 5a was located in northern California where major fuel types are mixed conifer forests with dominant species of ponderosa pine (*Pinus ponderosa*), Douglas fir (*Pseudotsuga menziesii*), and western hemlock (*Tsuga heterophylla*). The loading of the fuel types is heavier than that of other fuel types in California. At this fire polygon, the modified HANDS did an excellent job and the burnt area detected by it matched the CDF fire polygon almost exactly. The region mapped in Figure 5b was also located in northern California and contained another major fuel type, deciduous forests consisting of some oak woodland species (genus *Quercus*). From the overlaid result in Figure 5b, we see that the algorithm can detect the burnt area but fails to completely match the CDF fire polygon. This may lack a significant NDVI decrease, caused by the slight difference of

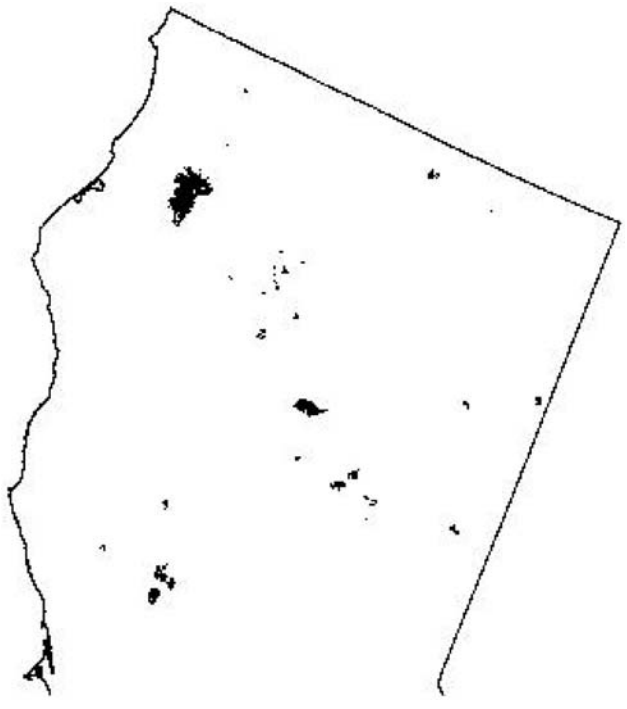

Figure 4. Burn scar map generated by the modified HANDS procedure for the 1999 fire season (May through October) in California. The region shown is the same as in Plate 1.

NDVI between burnt area and the phenological phase of senescence occurring in late fall for some deciduous species in California. Figure 5c represents a fuel type characterized by chaparral and Monterey pine (*Pinus radiata*), and was located near Monterey Bay, California. It also has greater biomass and fuel loading than fuel types represented in Figure 5b and 5d (scrub and grassland). The HANDS algorithm detected burned area not only over the CDF fire polygons, but linking neighboring polygons together as well. For the scrub and grassland fuel types (Figure 5d), the algorithm did its worst job, mapping approximately half the burnt area compared to the CDF polygon. This can be attributed to characteristics of the scrub and grassland ecosystems. If the scene is captured only at the end of the fire season, NDVI decrease may be insignificant due to the vegetation recovering fully or partially and burn scar detection can be constrained by this rapid re-vegetation (Eva and Lambin, 1998b). It is hoped that utilizing the iterative strategy (e.g., processing composites on a monthly basis) will help overcome the vegetation recovery problem (Fraser *et al.*, 2000).

Preliminary Validation

Only a small number of fire detection algorithms have been rigorously validated, due to the lack of ground truth data in most regions. In most cases, only cursory validations were conducted by comparing against fire smoke plumes (Li and Giglio, 1999). Therefore, validation of fire detection algorithms remains an outstanding issue. Since we did not have a complete set of ground truth data for validation, a preliminary validation was first carried out through human inspection of satellite composite images. Due to the sensitivity of channels 1 and 2 to fire smoke plume reflection, it is possible to use the composite image to visually inspect fires by their smoke. Comparing hotspot results detected by our method with their accompanying smoke plumes, we found that most hotspots detected had accompanying smoke plumes. This visual validation indicates that the modified fire detection algorithm is feasible.

Then, we conducted a simple statistical comparison between the results mapped with AVHRR data and CDF fire polygons. The AVHRR mapped burnt areas matching the CDF fire polygons were defined as follows. The area of all mapped fire polygons that intersect CDF polygons is calculated as the "matched" area. There is no minimum amount that polygons must intersect to be considered as matching. In this way, the statistical results were calculated and summarized in Table 4. Considering the high burnt area mapping rate and relative low commission and omission rates, the integrated approach is effective for mapping wildland fires in California. In addition, a more detailed validation of the burn scar maps with limited, comparable CDF fire polygons and TM interpreted polygon data was also carried out. For this case, twenty-seven fire polygons with recorded fire start date and acreages for 1999, provided by CDF and covering locations comparable to burnt areas detected by the modified HANDS algorithm were collected. TM images were first enhanced with traditional approaches, then, a standard false color composite image was made. Finally, eight corresponding and easily identified burnt areas were delineated from the three TM scenes. The fire polygons were compared with the burn scar map produced for the fire season by the modified HANDS procedure. The correspondence of burnt areas mapped with AVHRR data to the reference fire data is presented in Figure 6. The two sets of detected burnt areas are highly correlated ($R^2 = 0.83$). The overall agreement of burnt areas is 90.31 percent and the weighted average relative error is 37.42 percent ($\Sigma w_i|e_i| = 37.42$ percent, where w_i is area weight of i^{th} fire patch: the ratio between the area of the i^{th} fire patch and the total of all 35 fire polygons, e_i is the relative error of the i^{th} fire patch). This indicates that the results mapped by AVHRR are not ideal. However, if the reference data points are separated into CDF and TM groups, it is obvious that a better correlation can be found with the TM group ($R^2 = 0.97$, $n = 8$, solid line) than that from CDF group ($R^2 = 0.71$, $n = 27$, dashed line). The solid line associated with the TM group indicates that the burn scars detected with AVHRR are reliable, because the linear regression line is located near the diagonal line. This also implies that the CDF fire polygon data may not be as reliable as the TM data, although the number of interpreted burn scars from TM scenes is too small to enable a full comparison. From the thirty-five validated burnt areas, then, wildland fire seems detectable and able to be mapped, especially in forest ecosystems. Since the number of fire patches used for this validation is small, our preliminary results do not allow a full evaluation of the strength of the modified HANDS algorithm. A complete set of ground truth data, allowing independent validation among disparate fuel types (vegetation regions) is needed to evaluate these algorithms. Additional research is needed for analyzing burnt areas, mapped with remote sensing method, across eco-regional and eco-systematic boundaries and elucidating differences in the way fires are detected and mapped in different natural landscapes. The fire mapping results were described not only in terms of overall accuracy, but also in terms of divergent detection rates as they relate to on the ground differences in vegetation and land cover (Clinton *et al.*, 2004).

Conclusions

In order to map burnt areas in California for emission estimation, in this study, the Canadian Center for Remote

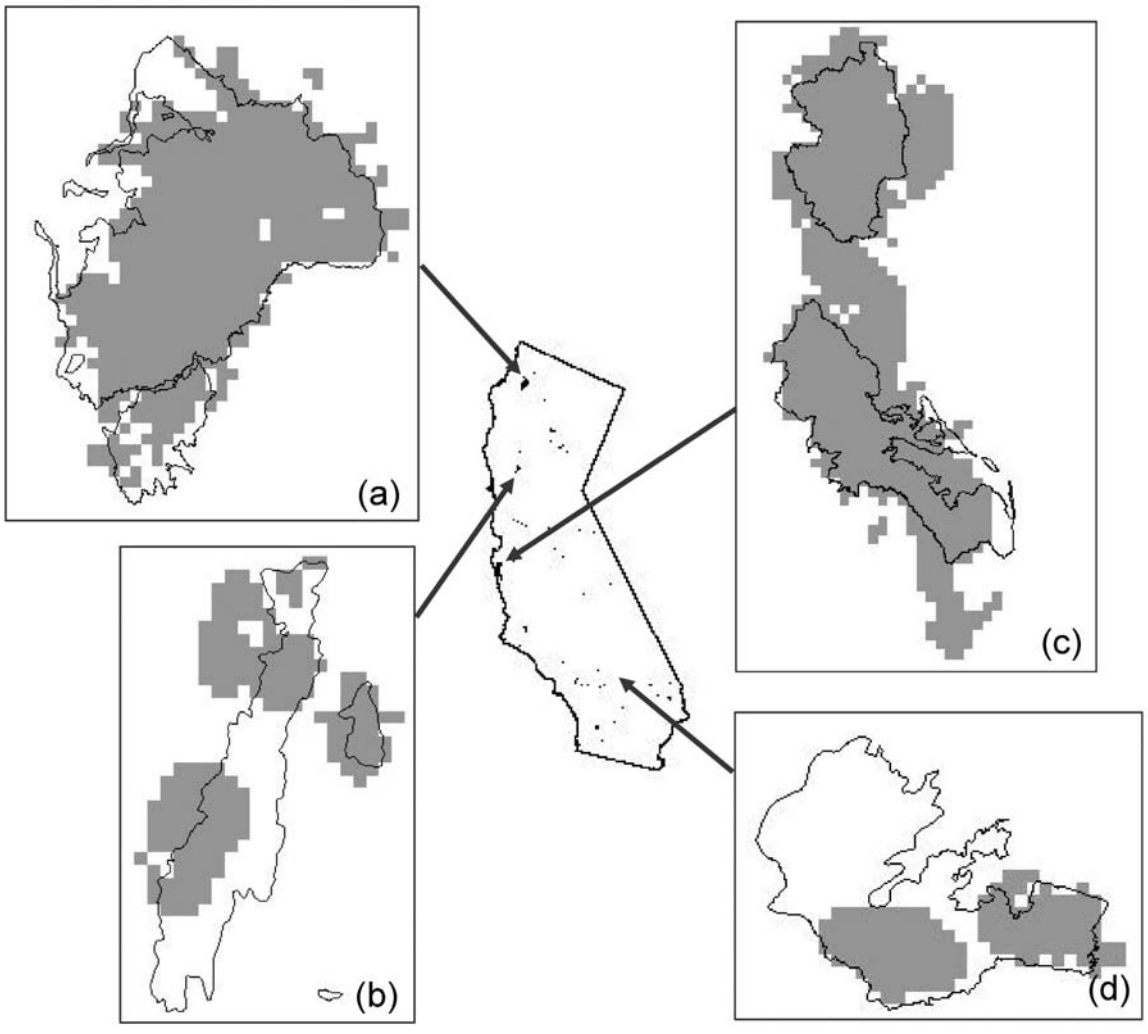

Figure 5. Using four major fuel types (ecosystems) in California to gain an insight into the burn scars detected by the modified HANDS algorithm. (a) Location in northern California with distribution of mixed conifer forests, fire mapped successfully; (b) location in northern California with deciduous forests, failed to match CDF fire polygon completely; (c) location near Monterey Bay and representing a fuel type with major species of chaparral and Monterey pine (*Pinus radiata*), fire over-detected; and (d) location in southern California with scrub and grassland ecosystems, fire much under-detected. The black lines in the figure represent fire polygon boundaries and the light shadow areas both inside and outside the polygons are burnt areas detected by the algorithm.

TABLE 4. A PRELIMINARY COMPARISON OF AVHRR MAPPED RESULT WITH CDF DATASET

Item	Burnt Area or Rate
AVHRR total burnt area mapped	3473 km^2
CDF fire polygons total burnt area	3204 km^2
AVHRR result matches CDF fire polygons	2502 km^2
AVHRR burnt area mapped rate	2502/3204 = 78.1%
Commission error rate	(3473–2502)/3204 = 30.3%
Omission error rate	(3204–2502)/3204 = 21.9%

Sensing (CCRS) active fire detection algorithm (Li *et al.*, 2000a) was first modified with the described additional contextual and sun glint tests, then applied to detecting daily hotspots in California using NOAA/AVHRR data acquired from 01 May to 31 October 1999. Finally, the HANDS procedure (Fraser *et al.*, 2000) was modified and applied to mapping burn scars in California with NDVI differencing and a hotspot mask covering a meaningful time period. The modifications to the HANDS algorithm include normalizing post-fire NDVI to pre-fire NDVI by multiplying an NDVI ratio coefficient, calculating the mean and SD of NDVI decrease of land cover types separately, and a new iteration procedure of confirming potential burnt pixels.

With this integrated hot spot detection and fire scar mapping technique and AVHRR data, wildland fires in California during the fire season between May and October in 1999 were mapped. Visual inspection of satellite composite images, validation with limited ground truth data from the California Department of Forestry and Fire Protection and the interpreted burnt areas from TM imagery revealed that most wildfires were correctly mapped, especially those

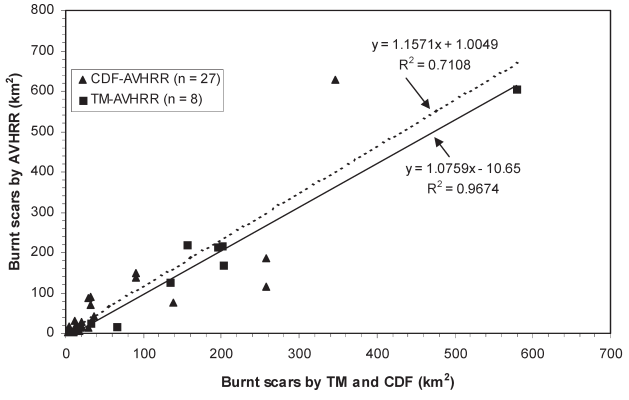

Figure 6. The relationship between the burnt areas delineated in TM scenes (eight fires in symbol square, regression analysis in solid line), those collected from CDF (27 fire polygons in triangle, regression analysis in dash line) and the corresponding burnt areas detected by the modified HANDS procedure.

in forest ecosystems. The extra tests added to the CCRS fire detection algorithm can effectively eliminate false fires caused by highly reflective clouds, sun glint, and warm backgrounds. Separating land-cover types, for the mean and standard deviation calculation of NDVI decreases in different vegetation types, allows us to discern burn scars from unburnt areas when they all have a temporal decrease in NDVI. In this experiment, the integrated method failed to map burnt areas with deciduous woodland, grass and shrub land ecosystems. To improve the effectiveness of fire detection over those ecosystems, a relatively short interesting time period for calculating NDVI difference is necessary to help overcome the vegetation recovery problem. For hotspot detection over grass and shrub lands, increasing frequency of satellite over-passes is needed.

The burnt areas (fire polygons) mapped with the integrated method using NOAA/AVHRR data were imported into an emission estimation system, designed specially for California (Scarborough *et al.*, 2001) and their outputs were evaluated. The integrated method of using remote sensing data for mapping burnt areas is promising for pollutant emission estimation at local to regional scales in terms of our preliminary test result by running the system.

Acknowledgments

This research was partially supported by the California Air Resources Board, a NASA land-cover and land-use grant, and an Overseas Distinguished Young Scientist Award of CAS, China.

References

Anderson, J.R., E.E. Hardy, J.T. Roach, and R.E. Witmer, 1976. A land use and land cover classification system for use with remote sensing data, *U. S. Geological Survey Professional Paper 964*, Washington, D.C., 28 p.

Arino, O., and J.M. Mellinotte, 1998. The 1993 Africa fire map, *International Journal of Remote Sensing*, 19: 2019–2023.

Arino, O., I. Piccolini, F. Siegert, H. Eva, E. Chuvieco, P. Martin, Z. Li, R.H. Fraser, E. Kasischke, D. Roy, J. Pereira, and D. Stroppiana, 1999. Burn scars mapping methods, *Forest Fire Monitoring and Mapping: A Component of Global Observation of Forest Cover, Report of a Workshop*, (F. Ahern, J-M Gregoire and C. Justice, editors), 03–05 November, Joint Research Centre, Ispra, Italy, pp. 198–223.

Boles, S.H., and D.L. Verbyla, 2000. Comparison of three AVHRR-based fire detection algorithms for interior Alaska, *Remote Sensing of Environment*, 72:1–16.

Clinton, N., P. Gong, and R. Pu, 2004. Evaluation of wildfire mapping with NOAA/AVHRR data by land cover types and ecoregions in California, *Geographic Information Sciences*, 10: 10–19.

Di, L., and D.C. Rundquist, 1994. A one-step algorithm for correction and calibration of AVHRR level 1b data, *Photogrammetric Engineering & Remote Sensing*, 60:165–171.

Dwyer, E., J.M. Gregoire, and J.P. Malingreau, 1998. A global analysis of vegetation fires using satellite images: Spatial and temporal dynamics, *Ambio*, 27:175–181.

Eva, H., and E.F. Lambin, 1998a. Remote sensing of biomass burning in tropical regions: Sampling issues and multisensor approach, *Remote Sensing of Environment*, 64:292–315.

Eva, H., and E.F. Lambin, 1998b, Burnt area mapping in central Africa using ATSR data, *International Journal of Remote Sensing*, 19:3473–3497.

Eva, H., and S. Flasse, 1996. Contextual and multiple-threshold algorithms for regional active fire detection with AVHRR data, *Remote Sensing Review*, 14:333–351.

Fernandez, A., P. Illera, and J.L. Casanoca, 1997. Automatic mapping of surfaces affected by forest fires in Spain using AVHRR NDVI composite image data, *Remote Sensing of Environment*, 60:153–162.

Flannigan, M.D., and T.H. Vonder Haar, 1986. Forest fire monitoring using NOAA satellite AVHRR, *Canadian Journal of Forest Research*, 16:975–982.

Flasse, S.P., and P. Ceccato, 1996. A contextual algorithm for AVHRR fire detection, *International Journal of Remote Sensing*, 17: 419–424.

Franca, J.R., J.M. Brustet, and J. Fontan, 1995, Multispectral remote sensing of biomass burning in West Africa, *Journal of Atmospheric Chemistry*, 22:81–110.

Fraser R.H., and Z. Li, 2002. Estimating fire-related parameters in boreal forest using SPOT VEGETATION, *Remote Sensing of Environment*, 82:95–110.

Fraser, R.H., Z. Li, and J. Cihlar, 2000. Hotspot and NDVI differencing synergy (HANDS): a new technique for burnt area mapping, *Remote Sensing of Environment*, 74:362–376.

Giglio, L., J.D. Kendall, and C.O. Justice, 1999. Evaluation of global fire detection using simulated AVHRR infrared data, *International Journal of Remote Sensing*, 20:1947–1985.

Harris, A.J.L., 1996. Towards automated fire monitoring from space: semi-automated mapping of the January 1994 New South Wales wildfires, *International Journal of Wildland Fire*, 6:107–116.

Holland, R.F., 1986. *Preliminary Descriptions of the Terrestrial Natural Communities of California*, State of California, The Resources Agency, Nongame Heritage Program, Department of Fish. and Game, Sacramento, California, 156 p.

Justice C., J.P. Malingreau, and A.W. Setzer, 1993. Remote sensing of fires: Potential and limitations, *Fire in the Environment* (P.J. Crutzen and J.G. Goldammer, editors), pp. 77–88.

Justice, C.O., and P. Dowty (editors), 1994. IGBP-DIS satellite fire detection algorithm workshop technical report, *IGBP-DIS Working Paper 9, NASA/GSFC*, Greenbelt, Maryland, February, 1993.

Justice, C.O., J.D. Kendall, P.R. Dowty, and R.J. Scholes, 1996. Satellite remote sensing of fires during the SAFARI campaign using NOAA advanced very high resolution radiometer data, *Journal of Geophysical Research*, 101:23851–23863.

Kasischke, E.S., and N.H. French, 1995. Locating and estimating the areal extent of wildfires in Alaskan boreal forests using multiple-season AVHRR NDVI composite data, *Remote Sensing at Environment*, 51:263–275.

Kasischke, E.S., and N.H. French, 1997. Constraints on using AVHRR composite index imagery to study patterns of vegetation cover in boreal forests, *International Journal of Remote Sensing*, 18: 2403–2426.

Kaufman, Y.J., C.O. Justice, L.P. Flynn, J.D. Kendall, E.M. Prins, L. Giglio, D.E. Ward, W.P. Menzel, and A.W. Setzer, 1998a. Potential global fire monitoring from EOS-MODIS, *Journal of Geophysical Research-Atmospheres*, 103: 32215–32238.

Kaufman, Y.J., R.G. Kleidman, and M.D. King, 1998b. SCAR-B Fires in the Tropics: Properties and their remote sensing from EOS-MODIS, *Journal of Geophysical Research*, 103:31955–31969.

Kaufman, Y.J., C.J. Tucker, and I. Fung, 1990. Remote sensing of biomass burning in the tropics, *Journal of Geophysical Research*, 95:9927–9939.

Kennedy, P.J., A.S. Belward, and J.M. Gregoire, 1994. An improved approach to fire monitoring in West Africa using AVHRR data, *International Journal of Remote Sensing*, 15:2235–2255.

Khazenie, N., and K.A. Richardson, 1993. Detection of oil fire smoke over water in the Persian Gulf region, *Photogrammetric Engineering & Remote Sensing*, 59:1271–1276.

Lee, T.M., and P.M. Tag, 1990. Improved detection of hotspots using the AVHRR 3.7 μm channel, *Bulletin of American Meteorological Society*, 71:1722–1730.

Li, Z., S. Nadon, J. Cihlar, and B. Stocks, 2000b. Satellite-based mapping of Canadian boreal forest fires: Evaluation and comparison of algorithms, *International Journal of Remote Sensing*, 21:3071–3082.

Li, Z., and L. Giglio, 1999. A review of AVHRR-based fire detection algorithms, *Forest Fire Monitoring and Mapping: A Component of Global Observation of Forest Cover, Report of a Workshop* (F. Ahern, J.M. Gregoire and C. Justice, editors), 03–05 November, Joint Research Centre, Ispra, Italy, pp. 175–197.

Li, Z., J. Cihlar, L. Moreau, F. Huang, and B. Lee, 1997. Monitoring fire activities in the boreal ecosystem, *Journal of Geophysical Research*, 102(D24):29611–29624.

Li, Z., S. Nadon, and J. Cihlar, 2000a. Satellite-based detection of Canadian boreal forest fires: Development and application of the algorithm, *International Journal of Remote Sensing*, 21: 3057–3069.

Li, Z., Y.J. Kaufman, C. Ichku, R. Fraser, A. Trishchenko, L. Giglio, J. Jin, and X. Yu, 2001. A review of AVHRR-based active fire detection algorithms: Principles, limitations, and recommendations, *Global and Regional Vegetation Fire Monitoring from Space: Planning and Coordinated International Effort* (A. Abern, J.G. Goldammer, and C. Justice, editors), SPB Academy. The Hague, pp. 199–225.

Malingreau, J.P., and C.O. Justice, (editors), 1997. *Definition and Implementation of A Global Fire Product Derived from AVHRR Data, 3rd IGBP-DIS Fire Working Group Meeting Report*, IGBP-DIS Working Paper 17, Toulouse, France, 13–15 November 1996.

Martin, M.P., and E. Chuvieco, 1995. Mapping and evaluation of burnt land from multitemporal analysis of AVHRR NDVI images, *EARSEL Advance Remote Sensing*, 4:7–13.

Muirhead, K., and A. Cracknell, 1985. Straw burning over Great Britain detected by AVHRR, *International Journal of Remote Sensing*, 6:827–833.

Pereira, J.M.C., 1999. A comparative evaluation of NOAA/AVHRR vegetation indexes for burned surface detection and mapping, *IEEE Transactions on Geosciences and Remote Sensing*, 37: 217–226.

Pereira, J.M.C., E. Chuvieco, A. Beudoin, and N. Desbois, 1997. Remote Sensing of Burned Areas: A Review, *A Review of Remote Sensing Methods for the Study of Large Wildland Fires* (E. Chuvieco, Editor) Departamento de Geografia, Universidada de Alcala, Alcala de Henares, pp. 127–184.

Pozo, D., E.J. Olmo, and L. Alados-Arboledas, 1997. Fire detection and growth monitoring using a multitemporal technique on AVHRR mid-infrared and thermal channels, *Remote Sensing of Environment*, 60:111–120.

Rauste, Y., E. Herland, H. Frelander, K. Soini, T. Kuoremaki, and A. RuKari, 1997. Satellite-based forest fire detection for fire control in boreal forests, *International Journal of Remote Sensing*, 18:2641–2656.

Razafimpanilo, H., R. Frouin, S.F. Iacobellis, and R.C.J. Somerville, 1995, Methodology for estimating burned area from AVHRR reflectance data, *Remote Sensing of Environment*, 54:273–289.

Scarborough, J., N. Clinton, R. Pu, and P. Gong, 2001. *Creating a Statewide Spatially and Temporally Allocated Wildfire and Prescribed Burn Emission Inventory Using Consistent Emission Factors*, Air Resources Board, California Environmental Protection Agency, pp. 1–55.

Setzer, A.W., and J.P. Malingreau, 1996. AVHRR monitoring of vegetation fires in the tropics: Toward the development of a global product, *Biomass Burning and Global Change*, (J.S. Levine, editor), The MIT Press, Cambridge, Massachusetts, London, England, pp. 25–39.

Setzer, A.W., and M.C. Pereira, 1991. Amazonian biomass burnings in 1987 and an estimate of their tropospheric emission, *Ambio*, 20:19–22.

Stroppiana, D., S. Pinnock, and J.M. Gregoire, 2000. The global fire product daily fire occurrence from April 1992 to December 1993 derived from NOAA AVHRR data, *International Journal of Remote Sensing*, 21:1279–1288.

(Received 03 September 2003; accepted 28 September 2004; revised 12 October 2004)